DELAMINATION GROWTH RATE IN COMPOSITE LAMINATES UNDER INCREASING LOW-VELOCITY IMPACT ENERGY

M. Francesca Pernice[1], Jiangning Gao[1] and Andrew T. Rhead[1,*]

[1] Department of Mechanical Engineering, University of Bath, Claverton Down, Bath, BA2 7AY, UK
[*] A.T.Rhead@bath.ac.uk

Keywords: Impact, damage, delamination, growth rate

ABSTRACT

Impact damage, and the reduction in strength it causes, continue to drive sizing of modern composite aircraft components. Despite the morphology of delaminations at interfaces near the non-impact surface of a laminate being critical to compression after impact failure and decades of research, computationally efficient, early-stage analytical design tools for calculating interface-by-interface damage do not yet exist. This study investigates, interface-by-interface, delaminations created by impact tests on carbon fibre/epoxy laminates with different quasi-isotropic stacking sequences each obtained from standard fibre angles. Fifty-three impact tests were performed with a 75mm circular test window under a range of impact energies providing results for 48 stacking sequences. Results show that the morphology of delamination caused by impact damage at each interface depends on the fibre angle of plies bounding the interface and is independent of stacking sequence or interface location within the stacking sequence. Conversely, the extent of delamination at each interface was found to vary with the location of the interface within the stacking sequence. Rate of growth of delamination with increasing impact energy is shown to vary with the difference in ply angle at an interface and some correlation is seen with through thickness distribution of bending and shear stresses during impact. This paper provides experimental data which can inform the development of models for damage development at interfaces near the non-impact surface of composite laminates subject to an impact event.

1 INTRODUCTION

Continuous fibre-reinforced polymeric composite laminates are susceptible to low-velocity impact damage. An impact event on the surface of a composite laminate often results in a small difficult to detect, surface dent referred to as "Barely Visible Impact Damage" (BVID). BVID typically causes extensive damage within the laminate, consisting of a complex pattern of delaminations at different ply interfaces, intra-laminar cracks and fibre failures [1, 2]. BVID resulting from a low-velocity impact event can be large enough to significantly reduce laminate strength. Compression after impact failures are often governed by sub-laminate buckling-driven delamination failures. Key to the prediction of such failures is the size of the delamination at each ply interface [3-6]. However, current analytical models [7, 8] for impact damage are not able to determine the size of individual delaminations, and numerical methods are often too computationally expensive to enable generic studies, which consider the multiple variables that affect delamination growth [9].

These difficulties in detecting impact damage and understanding its effect on strength means that the design of composite structures relies on oversizing of components to allow for reduced mechanical properties. The investigation of low-velocity impact damage is difficult as it depends on a number of different parameters, such as stacking sequence, laminate thickness, ply thickness, impactor geometry, impact energy and boundary conditions. Each combination of these parameters produces a unique damage morphology. Consequently, results obtained for a specific set of values for these parameters cannot be directly assumed to be valid for a different configuration. Therefore, a large number of experimental tests is needed to assess the impact resistance and post-impact performances of laminates with different stacking sequences.

In this work, the size of individual delaminations at each ply interface created by low-velocity impact events were measured experimentally. Laminates with different quasi-isotropic symmetric

stacking sequences and different number of plies were tested under a range of impact energies. Specimens were inspected using ultrasonic C-scan. The size of the delamination at each interface detected by the C-scan was measured in specimens at different energies. The rate of growth of the individual delaminations with impact energy was calculated and results for different stacking sequences compared.

2 EXPERIMENTAL

2.1 Stacking sequences selection

Low-velocity impact tests were conducted on specimens with various but comparable 16 and 24 ply quasi-isotropic symmetric stacking sequences obtained from standard fibre orientations (0°, ±45°, 90°), see Table 1. Stacking sequences were obtained from two basic sequences of four plies: *A* = (+45/ 0/ -45/ 90) and *B* = (+45/ -45/ 0/ 90). These two basic sequences differ in 'mismatch angle', the difference in angle between two plies bounding an interface. The mismatch angle is 45° at each interface in sequence *A* and 90° in two of the interfaces in sequence *B*, (+45/-45) and (0/90). Stacking sequences were obtained using the basic sequences *A* and *B* as building blocks in three different ways. The first method consisted of repeating a sub-laminate with layup equal to the basic sequence *A* or *B*. The stacking sequences obtained are labelled as type '*L*' (repeated Laminate) e.g. AM2_L16 in Table 1.

16-ply		24-ply	
Label	Stacking sequence	Label	Stacking sequence
AM2_L16	$[+45/0/-45/90]_{2S}$	AM2_L24	$[+45/0/-45/90]_{3S}$
AM2_P16	$[+45_2/0_2/-45_2/90_2]_S$	AM2_P24	$[+45_3/0_3/-45_3/90_3]_S$
AM2_OI16	$[(+45/0)_2/(-45/90)_2]_S$	AM2_OI24	$[(+45/0)_3/(-45/90)_3]_S$
BM2_L16	$[+45/-45/0/90]_{2S}$	BM2_L24	$[+45/-45/0/90]_{3S}$
BM2_P16	$[+45_2/-45_2/0_2/90_2]_S$	BM2_P24	$[+45_3/-45_3/0_3/90_3]_S$
BM2_OI16	$[(+45/-45)_2/(0/90)_2]_S$	BM2_OI24	$[(+45/-45)_3/(0/90)_3]_S$

Table 1: 16-ply and 24-ply quasi-isotropic symmetric stacking sequences for impact testing.

The second method consisted of stacking together two (for 16-ply stacking sequences) or three (for 24-ply stacking sequences) plies with the same fibre orientation in the basic sequences. The stacking sequences obtained are labelled as type '*P*' (repeated Ply) e.g. BM2_P24 in Table 1. Note that the outer eight plies in the stacking sequences AM2_P16 and BM2_P16 and the outer four plies in the corresponding stacking sequences AM2_L16 and BM2_L16 have the same sequence of interfaces, see Table 1. Comparison of results obtained from these two pairs of corresponding layups (AM2_L16, and AM2_P16, BM2_L16 and BM2_P16) allows the effect of ply thickness and through thickness interface position to be investigated in laminates of the same thickness.

The third method consisted of splitting each basic sequence into its two outermost (*O*) and two innermost (*I*) plies, (e.g. +45/0 and -45/90 for sequence *A*) and then repeating each pair. The stacking sequences obtained are labelled as type '*OI*' e.g. AM2_OI16 in Table 1.

2.2 Specimens' material and manufacturing

Specimens were obtained from 230-mm-wide and 170-mm-long panels, made using HTS40/977-2 carbon fibre/epoxy pre-preg, with material properties E_{11} = 153 GPa, E_{22} = E_{33} = 10.3 GPa, G_{12} = G_{13} = 5.2 GPa, G_{23} = 3.43 GPa, ν_{12} = ν_{13} = 0.3 and ν_{23} = 0.5 [10]. Two panels were manufactured for each stacking sequence. The panels were cured in an autoclave, according to the curing cycle recommended by the material manufacturer. Two specimens were obtained from each of the manufactured panels by trimming the edges of each panel and cutting them in half. Specimens were nominally 150 mm long (in the 0° fibre direction) and 100 mm wide (in the 90° fibre direction) [11], with an average cured thickness of 3.83 mm for the 16-ply specimens, and 5.88 mm for the 24-ply specimens, resulting in a cured ply thickness of 0.24 mm.

2.3 Low-velocity impact test method

Low-velocity impact tests were conducted at four energy levels, 6, 12, 18 and 24 J for the 16-ply specimens, and 12, 18, 24 and 30 J for the 24-ply specimens. Tests were performed using an Instron Dynatup 9250 drop weight impact tower, equipped with a 16 mm hemispherical tup. Tests were conducted according to the procedure outlined by the ASTM D7136 Standard Test Method [11], except for the geometry of the test window. Instead of the standard ASTM 125 mm × 75 mm rectangular test window [11], a test fixture with a 75-mm diameter circular impact window was used. The test fixture and a sketch of the impact specimen are shown in Fig. 1(a). Owing to rotational symmetry, use of a circular impact window allows damage morphologies for laminates with a 0°, 90° or -45° surface ply to be obtained with a single test of a laminate with a +45° surface ply, by rotating the delaminations at each interface. This is demonstrated in Fig. 1(b) for a +45/0 or a 90/+45 delamination. For this reason, only stacking sequences with +45° surface plies were tested.

One specimen of each stacking sequence was tested at each impact energy, except for the stacking sequences AM2_L16, AM2_L24 and BM2_P16. In these cases, two or three specimens were tested at each impact energy, in order to evaluate test repeatability for stacking sequences with single ply thickness (AM2_L16 and AM2_L24) and double ply thickness (BM2_P16).

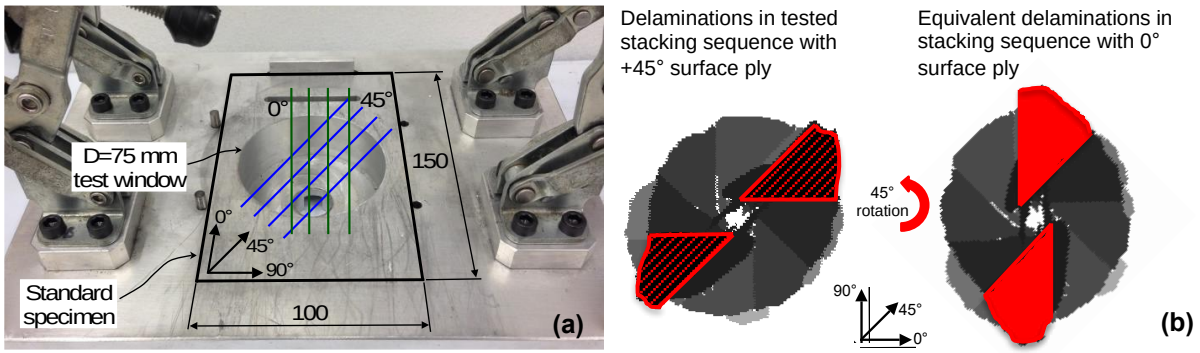

Figure 1: (a) Test fixture with circular test window and sketch illustrating the impact specimen and fibre orientation. (b) Schematic of the effect of the circular test window on delaminations in stacking sequences with rotated fibre orientations.

2.4 Inspection method

After testing, a 75-mm-square region of each specimen, centred on the impact location, was scanned using an Ultrasonic Sciences Ltd. C-scan system, equipped with a 35 MHz probe. Only the non-impact surface of each specimen was scanned. This is because the delaminations close to the non-impact surface are larger than on the impacted side and enable critical sub-laminate buckling-driven failures in a compression after impact loading scenario. The area of the specimens scanned corresponded to the 75-mm-diameter circular test window. For some specimens, the scanned area was extended to include delaminations that had grown beyond the boundary of the circular test window.

3 DELAMINATION SIZE MEASUREMENT

Typically, at each interface, delamination caused by impact is formed of two regions. Fig. 2 shows a Time-of-Flight (TOF) C-scan image of the non-impact surface of a specimen with stacking sequence AM2_L16. The two delaminated regions at each interface are clearly visible. In Fig. 2 interfaces close to the non-impact surface are identified by numbers 1, 2, 3 with 1 being closest to the surface.

The size of the delaminations at each interface was measured from the TOF C-scan images of the non-impact surface of the specimens. Measurements were taken using an automated Matlab code. In order to obtain measurements of interface-by-interface delaminations, the code recognises each interface as a different grey colour in the TOF image. The two delaminated regions at each interface are detected as regions of the image with the same colour, e.g. the two regions denoted 1 in Fig. 2 are

delaminations at the first +45/0 interface from the non-impact surface. For each delaminated region at each interface, the distance between the centre of impact and the point in each delaminated region at the greatest distance from the centre is measured. For some stacking sequences, at some interfaces, the two delaminated regions were highly asymmetric. To ensure conservatism the greater of the two distances at each interface was considered as representative of the maximum size of the delamination. In Fig. 2, for interfaces 1, 2 and 3, these points are marked by black 'x' symbols. Hereafter this measure is referred to as the "maximum delamination radius". This radius in general increases with increasing impact energy and is a measure of the length by which a delamination at a certain interface grows away from the centre of impact. However, it does not account for the actual delaminated area. As a result, a very narrow delamination, which extended at a great distance from the centre, will be associated to a greater delamination radius than a delamination which grows laterally but does not grow away from the centre of impact. Nevertheless, the maximum delamination radius is used herein as a measure of the size of the delamination at each interface.

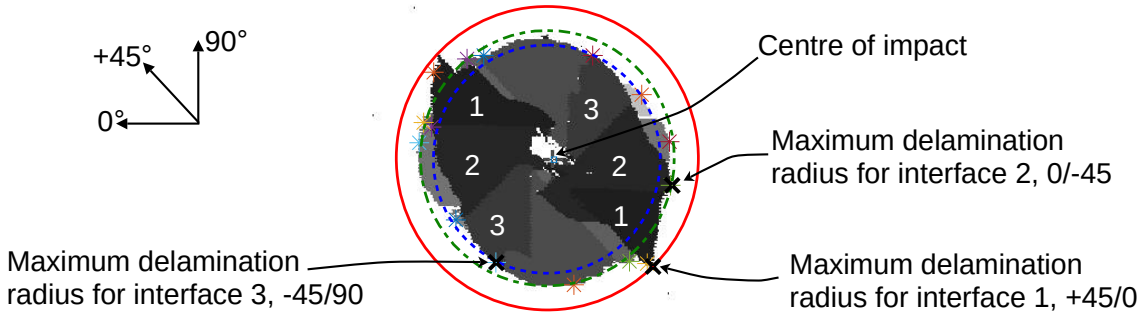

Figure 2: C-scan image of the non-impact surface of a specimen with stacking sequence AM2_L16 and circles having radius equal to the maximum delamination radius for the three delaminations closest to the non-impact surface.

4 RESULTS AND DISCUSSION

4.1 Delamination morphologies at each ply interface

Figures 3 and 4 show, for each of the 16-ply and the 24-ply stacking sequences respectively, a TOF image of the non-impact surface of a specimen impacted with 18 J. Interfaces are numbered starting from the non-impact surface. The images in Figs. 3 and 4 show that the shape (but not extent) of the delaminations at interfaces with the same orientation of bounding plies is the same, regardless of the overall stacking sequence, the location of the interface in the stacking sequence and the ply thickness. For instance, the first delamination in the stacking sequence AM2_L16 (Fig. 3) is located between a +45° and a 0° ply (interface 1) and is confined by the fibre orientation in the two bounding plies, +45° and 0°. All the other +45/0 interfaces have delamination of the same shape e.g. interface 5 in AM2_L16 and interface 3 in AM2_OI16 (Fig. 3). Delamination shape is also independent of laminate thickness, in fact delaminations shapes in the 24-ply specimens in Fig. 4 are the same as those in Fig. 3. For instance, the delaminations at the +45/0 interfaces in AM2_L24 in Fig. 4 (interface 5) have the same shape as the +45/0 interfaces in the 16-ply stacking sequences in Fig. 3.

Fig. 5 shows C-scan images of the non-impact surface of specimens with stacking sequence AM2_L16, tested at increasing impact energies. The image shows that the shape of the interface-by-interface delaminations remains the same as the impact energy increases. Comparison of the images in Fig. 5 reveals that the size of the individual delaminations increases with increasing impact energy. With increasing impact energy each delamination propagated along the fibre direction of the lower bounding ply. The same result was obtained for all the stacking sequences tested with both 16 and 24 plies. C-scan images of the other stacking sequences are omitted for brevity.

Comparison of Figs. 3 and 4 shows that for the 16-ply laminates near surface delaminations are marginally larger than near mid-plane delaminations. However, for the 24-ply laminates near mid-plane delaminations are larger indicating that peak shear stresses near the mid-plane play a more significant role in the propagation of delamination in the thicker laminates.

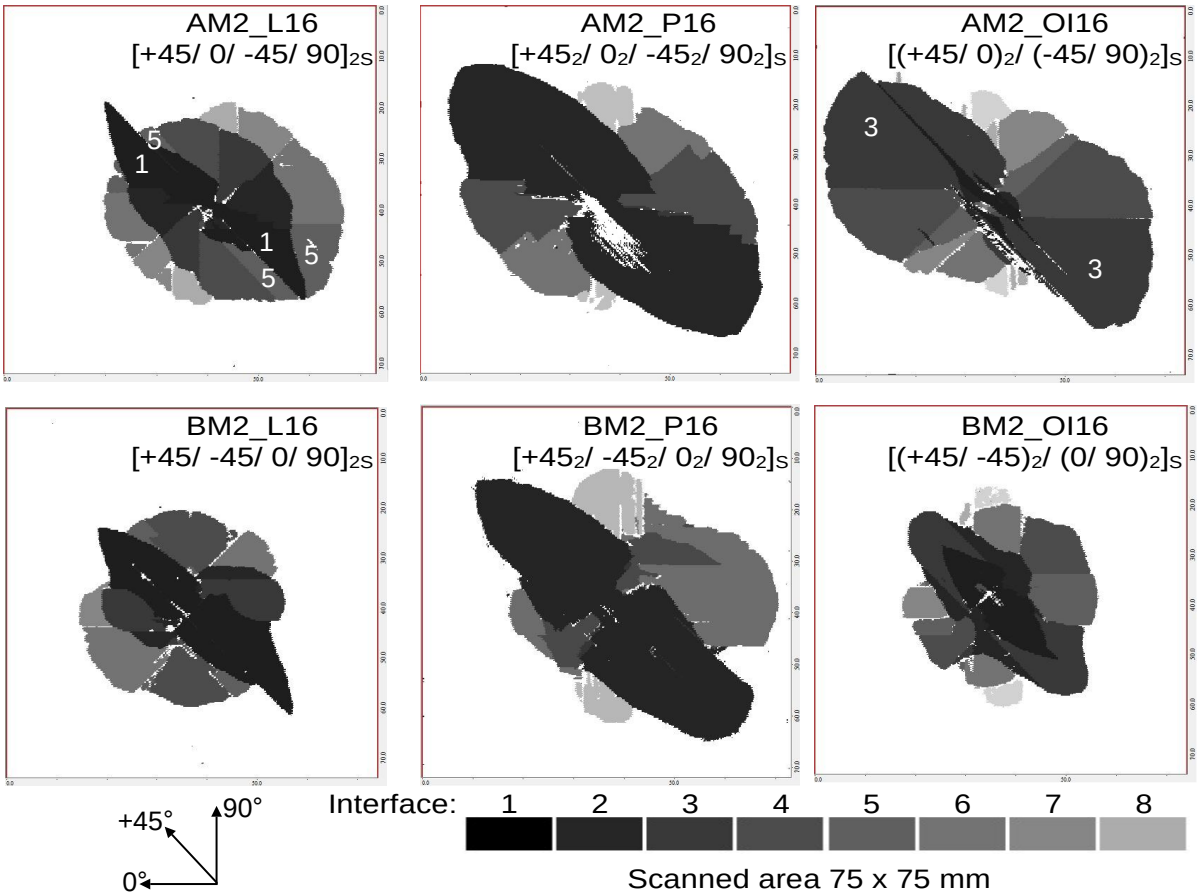

Figure 3: C-scan images of the non-impact surface of each of the 16-ply stacking sequences, after impact test at 18 J. Interfaces are numbered starting from the non-impact surface.

In a similar vein, Fig. 5 shows that near mid-plane delaminations dominate growth for higher impact energies. This indicates growth at higher energies is Mode II (shearing) driven as it occurs in through thickness regions associated with maximum shear stresses. Figures 6 and 7 show the maximum delamination radius plotted against the normalised distance of the interface from the non-impact surface for each 16-ply and 24-ply stacking sequence respectively. The distance of the interface from the non-impact surface of the specimen is normalised by the nominal thickness of the laminate, assumed to be 4 mm for 16-ply stacking sequences and 6 mm for 24-ply stacking sequences (nominal ply thickness of 0.25 mm). A normalised distance of 0 indicates the non-impact surface of the specimen, and a normalised distance of 0.5 indicates the position of the laminate mid-plane. Each graph in Figs. 6 and 7 represents a different stacking sequence. In each graph, the four curves indicate results obtained at the different impact energies tested, 6, 12, 18 and 24 J for 16-ply specimens and 12, 18, 24 and 30 J for 24-ply specimens. For the stacking sequences AM2_L16, AM2_L24 and BM2_P16, two or three specimens were tested at each impact energy, to evaluate test repeatability. Figs. 6 and 7 show the average values of the repeated tests. The average standard deviation in measurement of delaminations at each interface in repeated tests was 1.5 mm with a minimum standard deviation of 0.67 mm and maximum of 3.75 mm. In each plot, the horizontal line indicates the radius of the circular test window (37.5 mm). This value is shown as a limit for delamination size, since if a delamination grows past this value its growth is likely to be affected by the boundary condition in the test set up and should be treated with caution in the analysis of results.

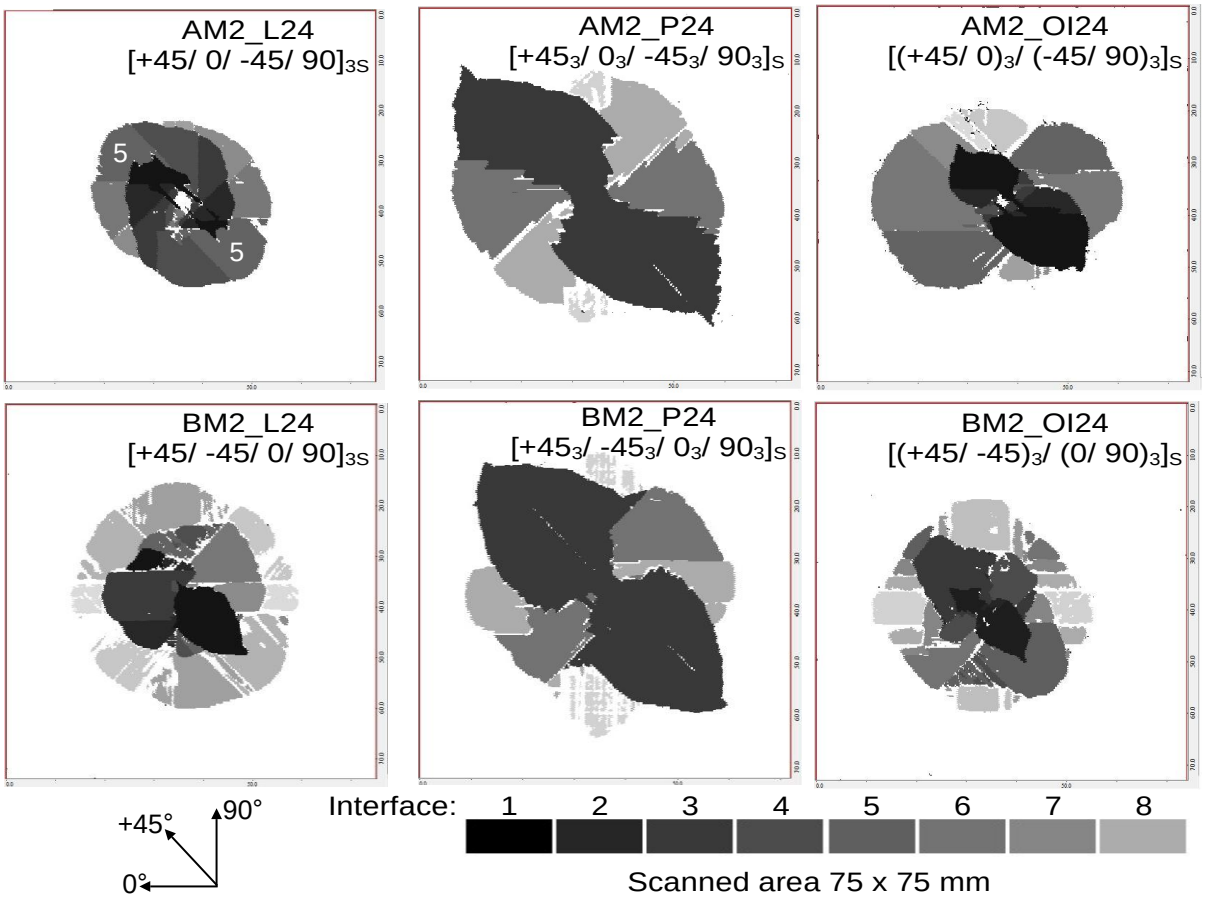

Figure 4: C-scan images of the non-impact surface of a specimen with each of the 24-ply stacking sequences, after impact test at 18 J. Interfaces are numbered starting from the non-impact surface.

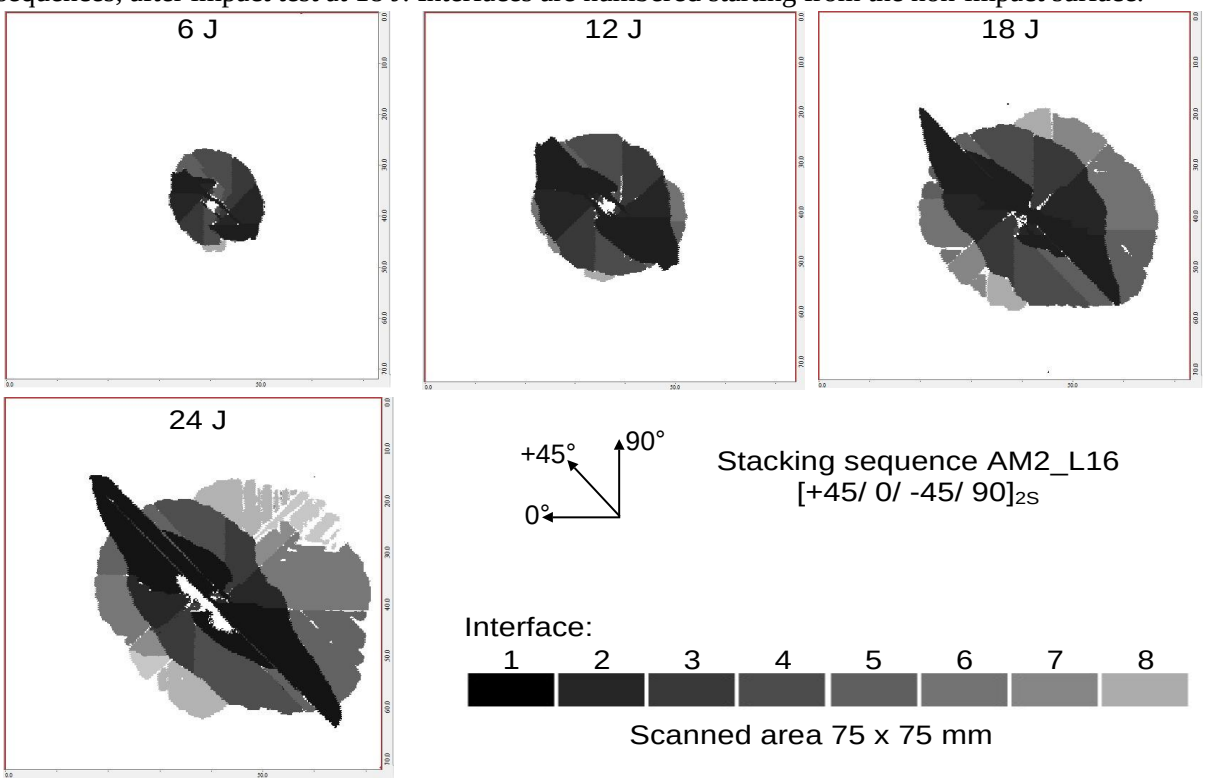

Figure 5: C-scan images of the non-impact surface of specimens with stacking sequence AM2_L16 tested at increasing impact energies. Interfaces are numbered starting from the non-impact surface.

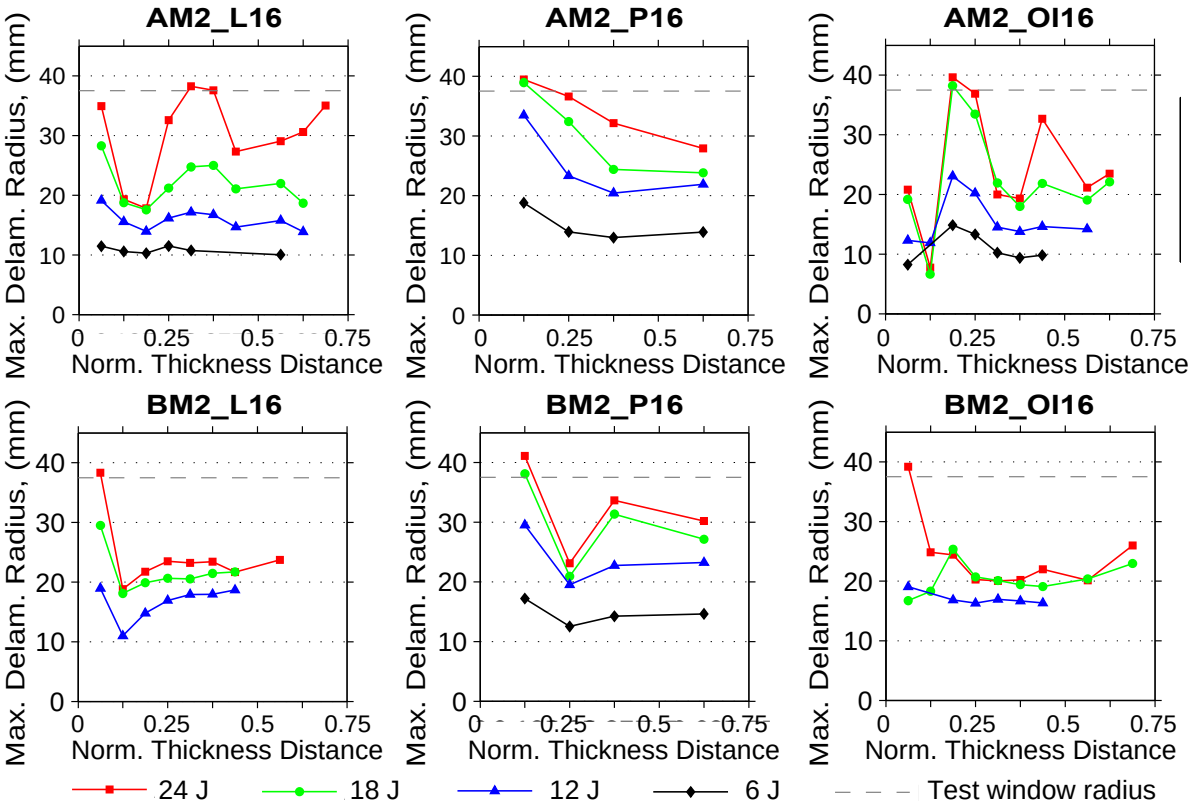

Figure 6: Maximum delamination radius plotted against the normalized through the thickness position of the interface at different impact energy, for all the 16-ply stacking sequences.

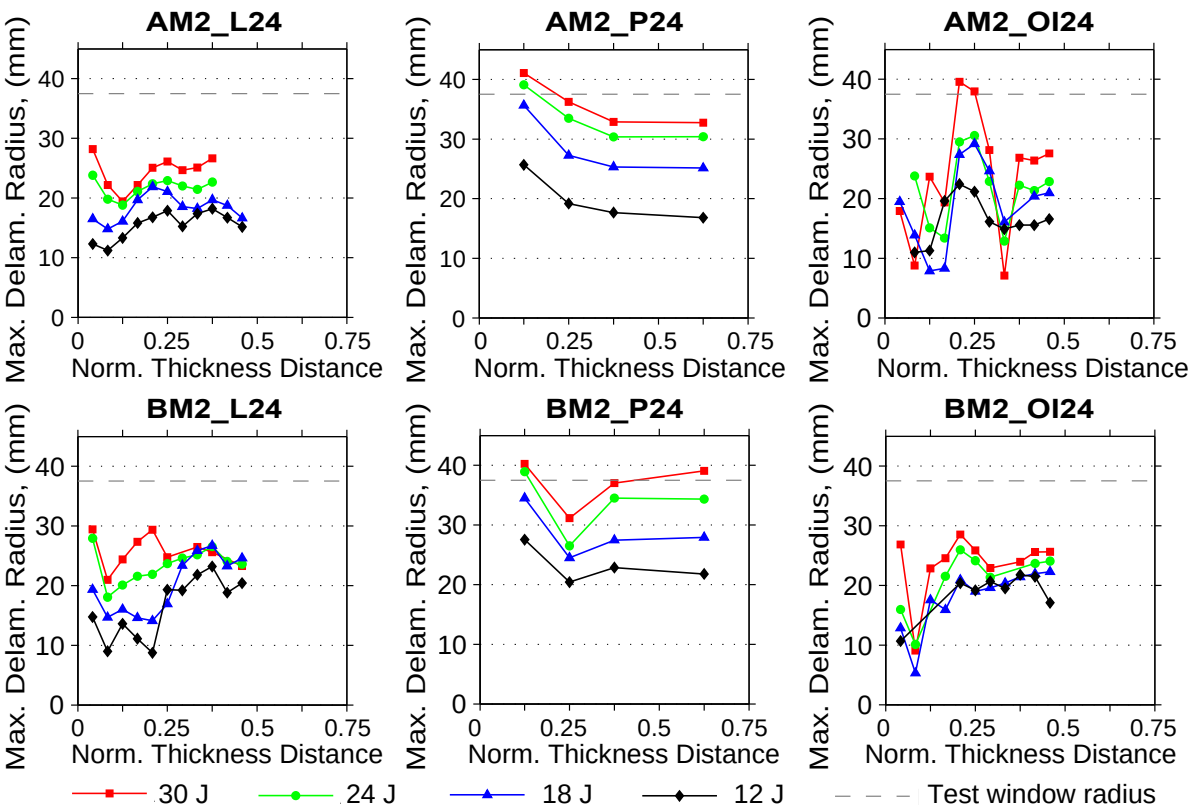

Figure 7: Maximum delamination radius plotted against the normalized through the thickness position of the interface at different impact energy, for all the 24-ply stacking sequences.

Figures 6 and 7 show that the maximum delamination radius measured for each delamination varies with the location of the delamination through the thickness of the laminate. The variation is different for each of the stacking sequences with the same number of plies. For each stacking sequence, the curves representing tests at different impact energies maintain similar shapes indicating a consistent damage morphology. Comparison of stacking sequences of the same type but with increasing number of plies, e.g. AM2_L16 and AM2_L24 and AM2_P16 and AM2_P24, shows a similar variation of the maximum delamination radius of the individual delaminations through the thickness of the laminates.

4.2 Delamination growth rate with energy

The rate of delamination growth with increasing impact energy was obtained from measurements of delaminations in laminates with the same stacking sequence tested at different impact energies. Comparison of curves for different impact energies in Figs. 6 and 7, shows that, in general, the rate of growth of delamination with energy is non-linear. Fig. 8 shows the maximum delamination radius as a function of the impact energy for all interfaces in specimens with stacking sequence BM2_P16. This graph is shown as representative of all the other stacking sequences tested. Fig. 8 shows a dashed line which gives a linear approximation to the curve for delamination radius vs. impact energy for the second interface. The slope of the linear approximation is taken to be the delamination growth rate for the interface.

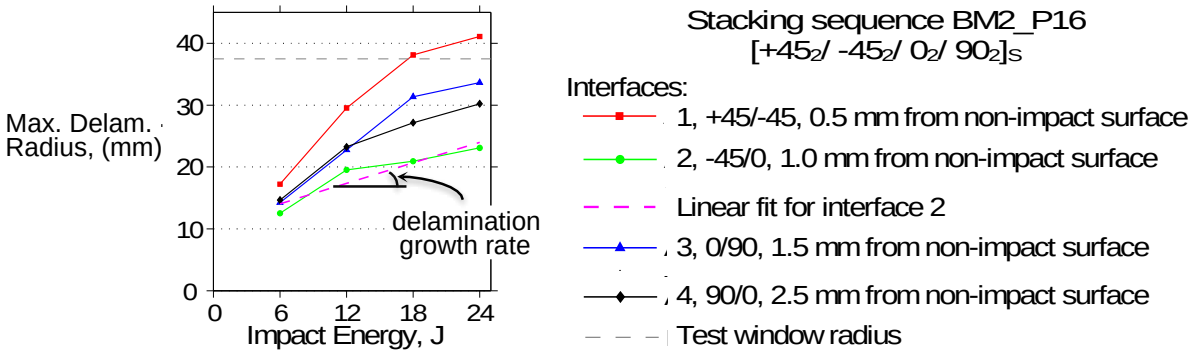

Figure 8: Maximum delamination radius as a function of impact energy for all the interfaces detected in specimens with stacking sequence BM2_P16. The plot shows the linear approximation used to calculate the delamination growth rate in case of the second interface from the non-impact surface.

The rates of growth of delamination at each interface as a function of the normalised distance from the non-impact surface for all sequences are shown in Fig. 9. The column on the left-hand-side shows all the 16-ply stacking sequences, the column on the right-hand-side shows the corresponding 24-ply stacking sequences. For stacking sequences of the same type but with different number of plies (each row in Fig. 9) the rate of growth of delamination varies as a function of the normalised through thickness location of the interface. For instance, for the two type '*L*' stacking sequences, AM2_L16 and AM2_L24, the rate of growth of delamination decreases after the first interface close to the non-impact surface and then increases again for a distance from the non-impact surface greater that 0.25 of the laminate thickness, see Fig. 9. For the stacking sequences with plies with the same fibre orientation stacked together (type '*P*'), the comparison is easier owing to there being fewer interfaces. Fig. 9 shows that the two stacking sequences AM2_P16 and AM2_P24 have maximum growth rate of delamination at a distance of 0.25 of the laminate thickness, while for the two stacking sequences BM2_P16 and BM2_P24 the interfaces located at 0.25 of the laminate thickness has the minimum growth rate. These two pairs of stacking sequences are of type $[+45_n/0_n/-45_n/90_n]_S$ (where *n* is the number of plies). These laminates have the same stacking sequence and the same number of interfaces but different ply and laminate thicknesses. Variation of delamination growth rate as a function of the normalized position of interface through thickness is also the same. The same is true for stacking sequences $[+45_n/ -45_n/ 0_n/ 90_n]_S$ (labeled as BM2_P16 and BM2_P24 in Fig. 9). This suggests that the rate of growth of delamination is independent of the ply thickness. However, if both the ply stacking

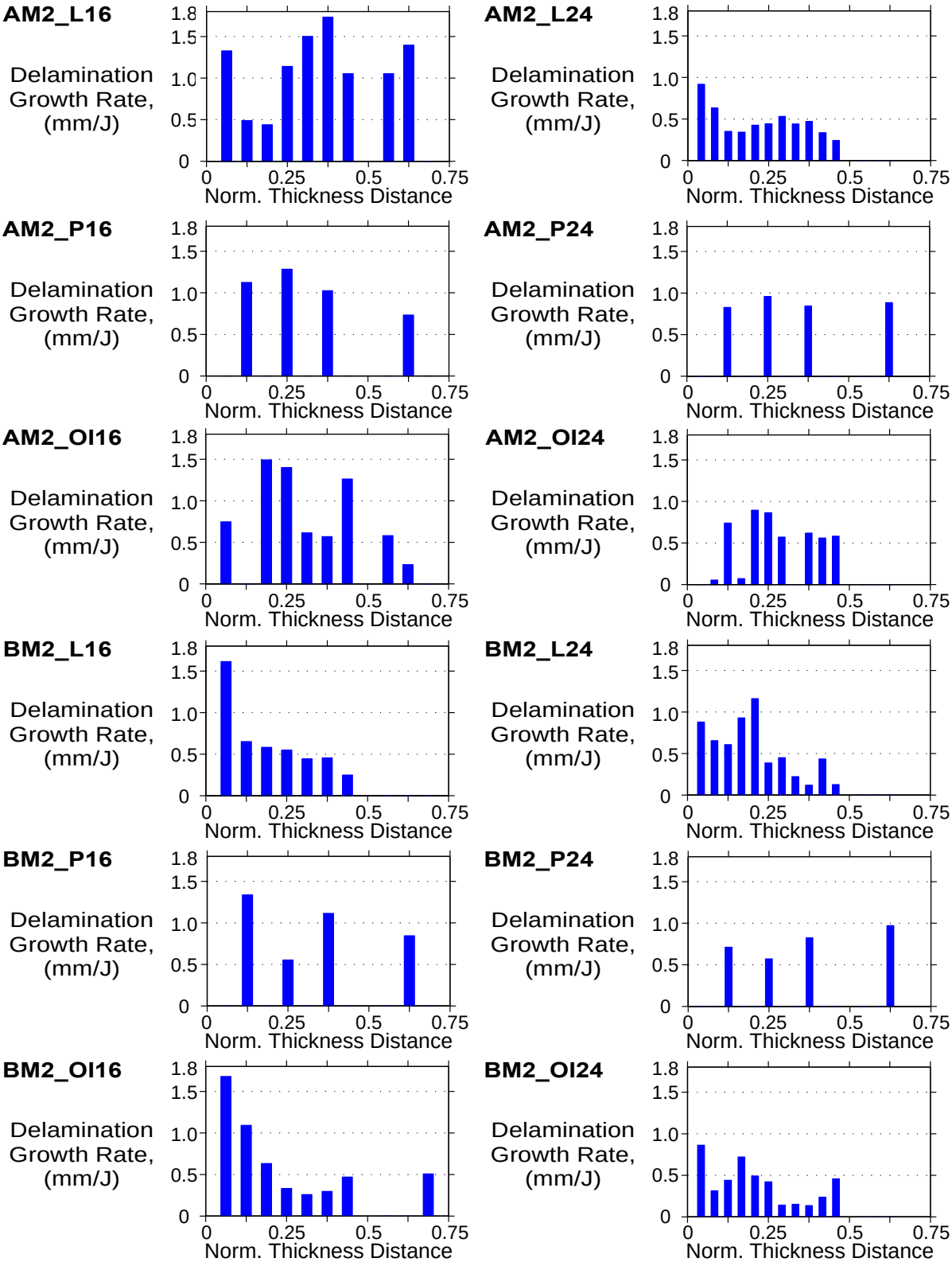

Figure 9: Rate of delamination growth with energy for each delamination as a function of the normalized through thickness position of the interface, measured from the non-impact surface of the specimen. Distance equal to 0.5 represents the laminate mid-plane.

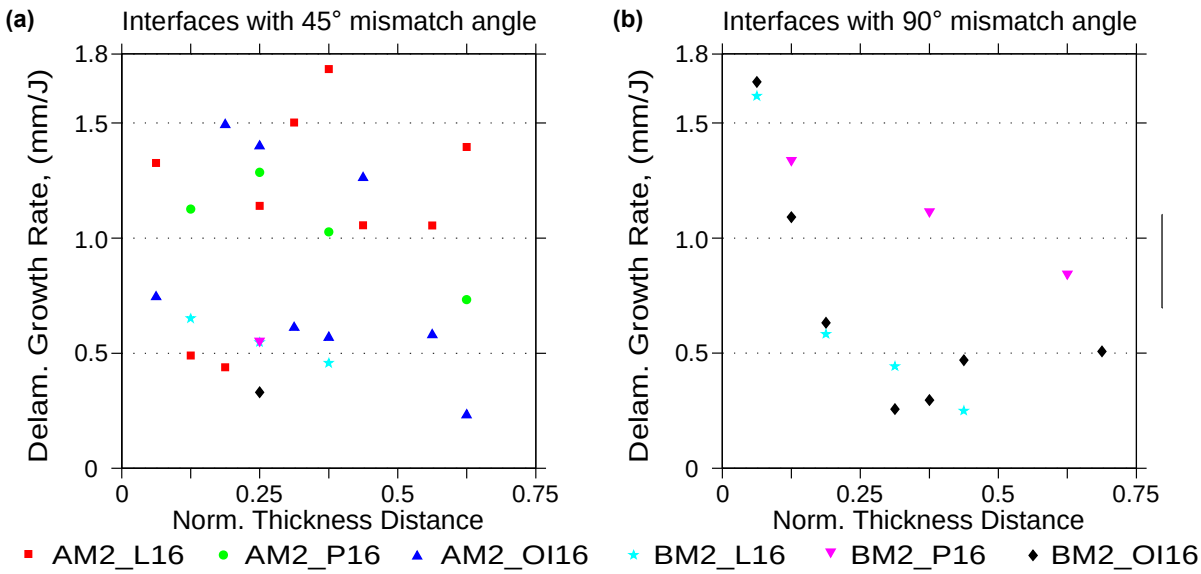

Figure 10: Delamination growth rate as a function of the normalised distance of the interface from the non-impact surface for all the interfaces in the 16-ply stacking sequences with 45° mismatch angle (a) and 90° mismatch angle (b).

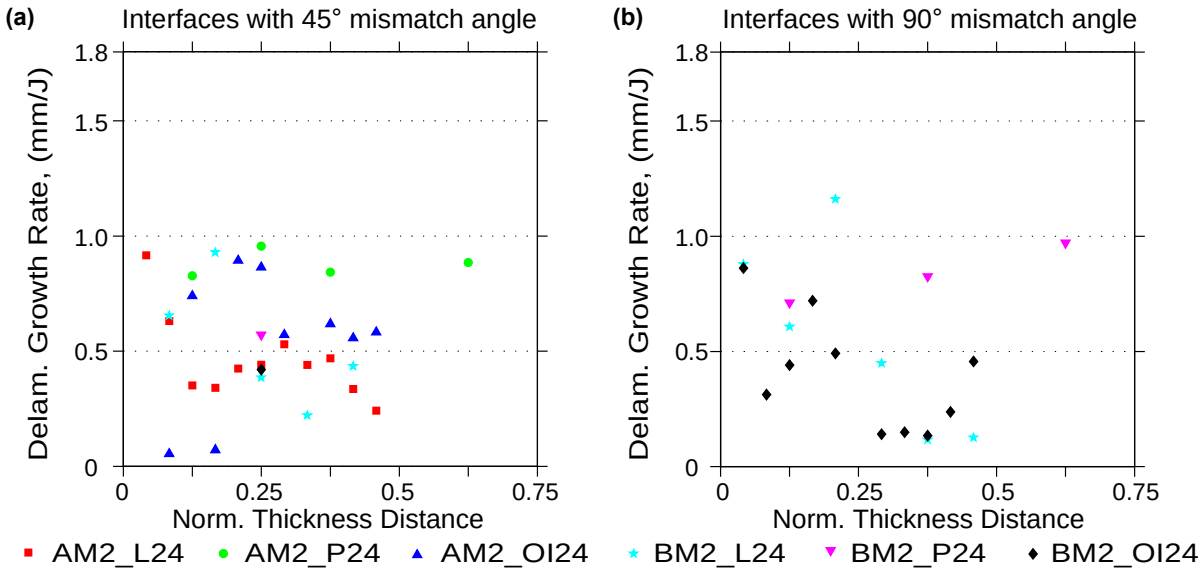

Figure 11: Delamination growth rate as a function of the normalised distance of the interface from the non-impact surface for all the interfaces in the 24-ply stacking sequences with 45° mismatch angle (a) and 90° mismatch angle (b).

sequence/number of interfaces are changed then the delamination growth rate is different. An example of this is given by stacking sequences $[+45/0/-45/90]_{2S}$ and $[+45_2/0_2/-45_2/90_2]_S$ (labeled as AM2_L16 and AM2_P16 in Fig. 9). Fig. 9 shows that in stacking sequence AM2_L16 the maximum delamination growth rate is at 0.375 of the laminate thickness, while it is at 0.25 of the laminate thickness for AM2_P16.

To better investigate the effect of the mismatch angle on delamination growth, the rate of growth for interfaces with a 45° mismatch angle and a 90° mismatch angle were plotted separately in Figs. 10 and 11, for the 16-ply and 24-ply stacking sequences respectively. Figs. 10(a) and 11(a) show the rate of growth of the individual delaminations for interfaces with 45° mismatch angle; the rate of growth of the individual delaminations is relatively uniform through the thickness of the specimen. Similarly, Figs. 10(b) and 11(b) show the rate of growth of the individual delaminations for interfaces with a 90°

mismatch angle. In general, with the exception of BM2_P24, the rate of growth of the individual delaminations is maximum for interfaces close to the non-impact surface of the specimens and decreases for interfaces close to the mid-plane of the laminate. This result can be ascribed to the through thickness shear stress distribution in the laminate resulting from the global bending of the specimen caused by impact and the local deformation below the indenter. Delaminated sublaminates formed near the non-impact surface of the specimen have fewer plies to offer mutual support that resists local deformation caused by the intact cylinder of material below the impinging indenter. Closer to the mid-plane of the laminate delaminated sublaminates are thicker and local bending deformation due to the indenter decreases. Instead shear stress increases and delamination propagation becomes shear dominated. Owing to the orthogonality of plies, interfaces with 90° mismatch angles can resist this Mode II (shear) driven delamination better than interfaces with a 45° mismatch angle. Therefore, the rate of growth of delamination decreases in the mid-plane region for interfaces with 90° mismatch angle (Figs. 10(b) and 11(b)). Interfaces with a 45° mismatch angle have a lower ability to resist to shear driven fracture and therefore the delamination growth rate is more uniform through the laminate thickness (Figs. 10(a) and 11(a).

5. CONCLUSIONS AND FUTURE WORK

Low-velocity impact tests were performed on specimens with various quasi-isotropic symmetric stacking sequences, derived from (+45/0/-45/90) and (+45/-45/0/90) ply blocks. Stacking sequences with 16 and 24 plies were obtained by repeating ply blocks, stacking together plies with the same fibre orientation or repeating two of the plies in the original ply block. Tests were performed at four impact energies.

It was found that the outline shape (but not extent) of individual delaminations depends only on the fibre orientation of the bounding plies and is independent of the stacking sequence, ply thickness, laminate thickness, location of the interface through the thickness of the laminate and impact energy. For each stacking sequence, as impact energy increases, delaminations grow along the fibre direction of the lower bounding ply.

The rate of growth of the delamination at each interface was calculated using a linear approximation to a delamination radius vs. impact energy curve. For all stacking sequences tested, the rate of growth of the individual delaminations varied with interface. It was found that stacking sequences of the same type have similar variation of the delamination growth rate through the thickness, independent of the laminate thickness (16-ply or 24-ply stacking sequences). The rate of growth of the individual delaminations can be linked to the interface mismatch angle. It was found that at interfaces with a 90° mismatch angle, the rate of growth of delamination decreases going from the non-impact surface towards the mid-plane of the laminate, thanks to the resistance to shearing (Mode II) fracture offered by the 90° mismatch angle. Conversely, interfaces with 45° mismatch angle have a lower ability to resist to Mode II fracture and therefore delamination growth rate does not significantly vary through the thickness of the laminate. A circular test window was used in this study, therefore it can be assumed that the fibre orientation of the lower ply at the interface does not affect the delamination growth rate.

Future work will include: results for 32 plies laminates derived from basic sequences *A* and *B*; quasi-static testing of zero-dominated laminates made from two carbon fibre/epoxy material systems, to allow comparison of delamination growth across materials; quasi-static impact of back-lit GFRP laminates to allow the connection between intra-laminar cracking and delamination formation to be understood.

ACKNOWLEDGEMENTS

This paper is part of the EPSRC founded project IMPACT (EP/M021270/1). The authors would like to thank Prof. Stephen Hallett (University of Bristol) for access to the impact test facilities at the University of Bristol.

REFERENCES

[1] A. Sandhu, L. Glen, M. Doughty, A. T. Rhead, X-Ray Computed Tomography of damage formation under in-situ loading. *Proceedings of the 20th International Conference on Composite Materials ICCM-20, Copenhagen, Denmark, July 19-24 2015.*

[2] E. Abisset, F. Daghia, X. C. Sun, M. R. Wisnom, S. R. Hallett, Interaction of inter- and intra-laminar damage in scaled quasi-static indentation tests: Part 1 – Experiments. *Composites: Part A*, **136**, 2016, pp. 712–726.

[3] R. Butler, A. T. Rhead, W. Liu, N. Kontis, Compressive strength of delaminated aerospace composites. *Philosophical Transactions of the Royal Society of London A*, **370**(1965), 2012, pp.1721-2026.

[4] A. T. Rhead, R. Butler, N. Baker, W. Liu, The influence of surface ply fibre angle on the compressive strength of composite laminates containing delamination. *Aeronautical Journal,* **116**(1186), 2012, pp.1315-1330.

[5] A. T. Rhead, R. Butler, G, W. Hunt, Post-buckled propagation model for compressive fatigue of impact damaged laminates. *International Journal of Solids and Structures,* **45**(16), 2008, pp.4349-4361.

[6] A. T. Rhead, R. Butler, Compressive static strength model for impact damaged laminates. *Compos. Sci. Technol.,* **69**(14), 2009, pp.2301-2307.

[7] R. Olsson, Closed form prediction of peak load and delamination onset under small mass impact. *Composite Structures*, **59**, 2003, pp. 341–349.

[8] R. Olsson, M. V. Donadon, B. G. Falzon, Delamination threshold load for dynamic impact on plates. *International Journal of Solids and Structures*, **43**, 2006, pp. 3124–3141.

[9] C. Bouvet, B. Castanie, M. Bizeul, J. J. Barrau, Low-velocity impact modelling in laminate composite panels with discrete interface elements. *International Journal of Solids and Structures*, **46**(14-15), 2009, pp. 2809–2821.

[10] A. Atas, C. Soutis, Strength prediction of bolted joints in CFRP composite laminates using cohesive zone elements. *Composites: Part B*, **58**, 2014, pp. 25-34.

[11] ASTMD7136/D7136M-15. Standard Test Method for Measuring the Damage Resistance of a Fiber-Reinforced Polymer Matrix Composite to a Drop-Weight Impact Event. In Annual Book of ASTM Standards, volume 15.03. American Society for Testing and Materials, 2015.